Available online at www.sciencedirect.com

ScienceDirect

journal homepage: www.elsevier.com/locate/he

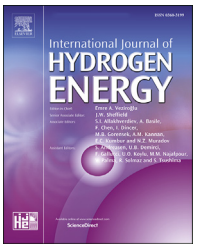

Estimation of system-level hydrogen storage for metal-organic frameworks with high volumetric storage density

Justin Purewal [a], *Mike Veenstra* [a], *David Tamburello* [b], *Alauddin Ahmed* [c], *Adam J. Matzger* [d], *Antek G. Wong-Foy* [d], *Saona Seth* [d], *Yiyang Liu* [d], *Donald J. Siegel* [c,*]

[a] *Ford Motor Company, Research and Advanced Engineering, 1201 Village Rd, Dearborn, MI 48121, USA*
[b] *Savannah River National Laboratory, Aiken, SC 29808, USA*
[c] *Mechanical Engineering Department, University of Michigan, Ann Arbor, MI 48109, USA*
[d] *Department of Chemistry, University of Michigan, Ann Arbor, MI 48109, USA*

ARTICLE INFO

Article history:
Received 28 February 2019
Received in revised form
29 March 2019
Accepted 9 April 2019
Available online 3 May 2019

Keywords:
hydrogen storage
Metal-organic-framework
Cryo-adsorption
Adsorbent

ABSTRACT

Metal organic framework (MOF) materials have emerged as the adsorbent materials with the highest H_2 storage densities on both a volumetric and gravimetric basis. While measurements of hydrogen storage at the material level (primarily at 77 K) have been published for hundreds of MOFs, estimates of the system-level hydrogen storage capacity are not readily available. In this study, hydrogen storage capacities are estimated at the system-level for MOFs with the highest demonstrated volumetric and gravimetric H_2 storage densities. System estimates are based on a single tank cryo-adsorbent system that utilizes a type-1 tank, multi-layer vacuum insulation, liquid N_2 cooling channels, in-tank heat exchanger, and a packed MOF powder inside the tank. It is found that with this powder-based system configuration, MOFs with ultra-high gravimetric surface areas and hydrogen adsorption amounts do not necessarily provide correspondingly high volumetric or gravimetric storage capacities at the system-level. Meanwhile, attributes such as powder packing efficiency and system cool-down temperature are shown to have a large impact on the system capacity. These results should shed light on the material properties that must to be optimized, as well as highlight the important design challenges for cryo-adsorbent hydrogen storage systems.

Introduction

Fuel cell vehicles store hydrogen on-board as a 700 bar compressed gas in expensive and bulky pressure vessels. An alternative hydrogen storage method is to pack high-surface area adsorbents into low pressure tanks (roughly 7 times lower) which need to be maintained at cryogenic temperatures [1]. There are numerous benefits to this approach, including a lower working pressure which enables the use of

* *Corresponding author.*
E-mail address: djsiege@umich.edu (D.J. Siegel).
https://doi.org/10.1016/j.ijhydene.2019.04.082

lower-cost type-1 tanks [2]. Further, cryo-adsorption systems would take full advantage of a liquid hydrogen infrastructure pathway, in which hydrogen fuel is delivered as a cryogenic liquid, which would potentially be more efficient for high-volume delivery and usage rates [3].

Many adsorbent materials have been studied to evaluate their potential storage capability, ranging from activated carbons to highly tunable metal-organic frameworks (MOF) [4–7]. Interestingly, the well-known metal-organic framework, $Zn_4O(BDC)_3$ (known as MOF-5 and/or IRMOF-1), is still considered as a benchmark material for hydrogen adsorbents with high gravimetric and volumetric capacities [8]. However, further improvements to the hydrogen storage capacities of adsorbents are required in order to match and surpass 700 bar compressed storage. In particular, the design and testing of sub-scale cryo-adsorbent systems based on MOF-5 has revealed that volumetric capacity (i.e., the mass of hydrogen stored within a specific volume) is a key material property of adsorbents which currently limits system performance [9]. Recently synthesized MOFs now have BET surface areas exceeding 5000 m^2g^{-1} and 77 K excess hydrogen adsorption amounts higher than 8 wt% [10–12]. However, the low crystal densities of these MOFs may limit or negate any corresponding increase in volumetric capacity [13]. Inefficient packing of low-density MOF powders within sorbent beds further erodes volumetric capacity.

Between 2009 and 2015 the Hydrogen Storage Engineering Center of Excellence (HSECoE) designed and built two sub-scale prototypes of a cryo-adsorption hydrogen storage system that utilized MOF-5 as the adsorbent [2,9]. Design details and performance data that emerged from these prototypes were used to develop a model that calculates the gravimetric and system storage capacities for a full scale cryo-adsorbent system with 5.6 kg of usable hydrogen [14]. Initial estimates (based on conservative assumptions for material-level MOF-5 properties) indicated that a cryo-adsorbent system was actually close to matching a 700 bar compressed system in terms of volumetric capacity [15]. Based on these findings, MOFs with moderately improved hydrogen storage capacities have the potential to surpass 700 bar compressed H_2 storage at the system level [13].

In this report we have evaluated the hydrogen adsorption properties for a number of high-surface-area MOFs identified through computational screening as having the potential of surpassing MOF-5 in both volumetric and gravimetric storage capacity [16]. Further, the effect of compaction density on hydrogen storage capacity is characterized for a number of the top performing MOFs. Material-level hydrogen storage properties are then incorporated into a system model in order to estimate the hydrogen storage capacity at the system-level. The results illustrate the benefits of systems based on highly-compacted MOF monoliths rather than on loose-packed powders. Based on these findings, strategies are discussed for improving the system-level volumetric storage capacity.

Experimental methods

MOF synthesis

Synthesis methods for MOFs closely follow previously published methods for IRMOF-20 [17], SNU-70 [18], DUT-23 (Co) [19], UMCM-9 [20] and NU-100 [10]. Details on the synthesis of MOF-5, IRMOF-20 and DUT-23 (Co) are available in Ref. [16]. Similar details for the synthesis and activation of UMCM-9 and NU-100 are described in Ref. [21].

BET surface area

Nitrogen BET surface areas were measured (Micromeritics ASAP2420) for each MOF following H_2 adsorption isotherms. Sample loading was performed inside a high-purity argon glovebox. Before transferring it out of the glovebox, a glass filler rod was inserted in the sample cell, and a seal frit with rubber O-ring was used to seal off the sample cell and prevent exposure to moisture. Free space was calculated from the previously measured values for an empty sample cell and the measured sample skeletal density (typically measured during H_2 adsorption measurements).

The measured BET surface areas of microporous MOFs, when calculated according to the consistency criteria in Ref. [23], have been shown to be consistent with the physical surface areas computed from molecular models of the defect-free MOF crystal structure [24]. Therefore, the BET consistency criteria were used to select the range of N_2 adsorption data points fitted to the BET model. For transparency, plots of N_2 adsorption isotherms and the fits to the BET model are available for each sample in the Supporting Information document.

Excess hydrogen adsorption

Hydrogen excess supercritical adsorption and desorption measurements were performed using a manometric Sievert's-type instrument (HPVA-2, Micromeritics [25]) connected to a turbomolecular vacuum pump with an oil-free diaphragm backing pump. The HPVA-2 system was regularly validated by empty cell measurements and reference material measurements [26], along with participation in an inter-laboratory study. Additional details on the adsorption measurement methods are in Ref. [16]. Plots of the excess H_2 adsorption isotherms for individual MOFs at powder density are available in the Supporting Information document.

Defining the free space in the sample cell requires knowing the skeletal density (ρ_{sk}) of the sorbent, which can be thought of as the hard volume which is impenetrable to helium (and hydrogen) gas. For a porous material this can include closed pores which even H_2 molecules cannot reach, but does not include inter-particle, inter-granular or inter-crystallite spaces. The free space is defined as

$$V_{fs} = V_{ext} - \frac{m}{\rho_{sk}} \quad (1)$$

where V_{ext} is the geometrical volume of interest (which could be the volume of the empty sample cell, or the volume of a hypothetical single crystal sample of MOF, or the geometrical volume of a pellet), and m is the mass of sorbent loaded in the sample cell. Excess adsorption is equal to the amount of gas present in the free space minus the amount of gas which would be present in that same volume if it were at the gas density (ρ_{gas}). Therefore, the excess adsorption is the extra amount of the gas present in the sample cell due to the enhanced hydrogen gas density within the sorbent pores.

Free space measurements were performed using helium at room temperature to estimate the internal volume of an empty sample cell. Similarly, the skeletal density (ρ_{sk}) of the microporous samples was measured by helium expansion only at room temperature to avoid errors arising from helium adsorption.

Hydrogen adsorption measurements were primarily performed at low sample temperatures with the sample cell immersed in a cryogenic bath. In this case, the sample cell volume was divided into two temperature zones: an ambient temperature zone at room temperature and a cold temperature zone immersed in the cryogenic bath. The ambient zone volume and cold zone volume of an empty sample cell were measured with the cryogenic bath filled to a marked level on the sample cell (which remained unchanged from measurement to measurement). After loading samples, the ambient and cold free space values were calculated by subtracting the skeletal volume (i.e., $V_{sk} = m/\rho_{sk}$) from the empty sample cell volumes. A porous polymer Isothermal Jacket™ supplied by Micromeritics was strapped onto the sample stem to mitigate temperature fluctuations arising from evaporation of the cryogenic liquid and the gradual lowering of the liquid level.

Hydrogen adsorption isotherms were measured at four temperatures using cryogenic liquid baths (77 K, 87 K), solvent slush baths (195 K) and ambient temperature (298 K). Temperature was measured using a platinum resistance thermometer which was calibrated at three temperatures (77 K, 273 K and 298 K). To maintain a sample temperature of 195 K, the sample cell was immersed in a slurry prepared from solid CO_2 dry ice granules and isopropanol. Large pellets of dry ice were ground up into small granules and then mixed throughly with isopropanol in a small beaker. Successive batches were then transferred to a dewar until the slurry level reached the required height on the sample cell stem. The temperature of the slurry remained steady within ±0.1 K during the span of the measurement.

Hydrogen adsorption measurements at variable MOF packing densities were performed by compacting the MOF sample directly within the sample cell to successively higher densities. The internal diameter of the sample cell was 4.6 mm and the internal depth was 39.4 mm. Powder MOF samples were loaded in the sample cell inside the glovebox and compacted to a specified density using a 4.5 mm outer diameter pellet press. The same MOF sample was used for successive measurements without loading fresh MOF. The packing densities of the MOF were measured before and after each measurement and no change in density was detected. Skeletal density was measured only for the MOF at powder density and was assumed to not change as a result of compaction. While the skeletal density may decrease due to the formation of closed pores, the adsorption instrument as configured did not have the accuracy to detect such a small change in volume.

Total hydrogen storage

Total hydrogen volumetric and gravimetric capacities were calculated following recommended methods provided in Ref. [27]. The total adsorption is equal to the excess adsorption plus the H_2 present at normal gas density within the free space. Referring to Eq. (1), the external volume can be equal to the MOF crystal volume ($V_{ext} = m/\rho_{crystal}$), or it could be equal to the geometrical volume enclosing a packed powder ($V_{ext} = m/\rho_{pwd}$) or compacted pellet ($V_{ext} = m/\rho_{pellet}$). For generality, it is assumed that the external volume is defined by some type of sorbent packing density (ρ_x).

The amount of H_2 (in grams) stored per 1 L of sorbent (total volumetric storage) is

$$n_v = \rho_x n_{ex} + \rho_{gas}\left(1 - \frac{\rho_x}{\rho_{sk}}\right). \tag{2}$$

For Eq. (2) to yield volumetric capacity in units of g/L, the skeletal (ρ_{sk}) and sorbent density (ρ_x) are both written in kg/L, while the bulk H_2 gas density, ρ_{gas}, is expressed in g/L. Meanwhile, the excess adsorption n_{ex} is expressed in units of g/kg (grams H_2 per kg sorbent).

Material-level volumetric capacities are calculated from Eq. (2) using the MOF crystal density $\rho_x = \rho_{crys}$. The argument in favor of using the MOF crystal density rather than the practical powder packing density is that the crystal density reflects an intrinsic material property, making it more appropriate for comparisons between different MOFs [28]. However, as discussed in Sec. System model it is the powder packing properties of MOFs that actually have a more significant impact on the practical system-level storage capacities. The total gravimetric storage capacity in wt. % may be calculated from the volumetric storage capacity,

$$n_g = \frac{n_v}{n_v + 1000 \cdot \rho_x} \times 100, \tag{3}$$

which follows the convention of including the combined mass of the adsorbent material and the stored hydrogen in the denominator.

Usable capacity

The pressure swing (PS) hydrogen storage capacity is equal to the difference between the 77 K volumetric H_2 storage at 100 bar and 5 bar. In other words, hydrogen below 5 bar is defined as not usable for delivery to the fuel cell system without heating the MOF. The hydrogen storage system therefore is assumed to be isothermal, although during system operation heating should be available from either heat transfer through the tank insulation, or from internal heating (resistive heating or heat exchanger connected to the fuel cell coolant system). The PS capacity at $T = 77$ K for MOF-5 is illustrated in the left panel of Fig. 1.

The second material-level capacity definition is based on the temperature and pressure swing (TPS) process [29]. In this case, the capacity is the difference between hydrogen volumetric capacity at a full state of 100 bar, 77 K state and an empty state of 5 bar and 160 K. An upper temperature of 160 K is chosen because it provides a compromise between maximizing the usable H_2 capacity while at the same time maintaining an acceptable cool-down time to 77 K during refilling. Fig. 1 illustrates the distinction between PS and TPS capacity using published MOF-5 data from Ref. [22] as an example. The TPS capacity is clearly larger than the PS capacity owing to the lower concentration of hydrogen that is retained at 160 K versus 77 K.

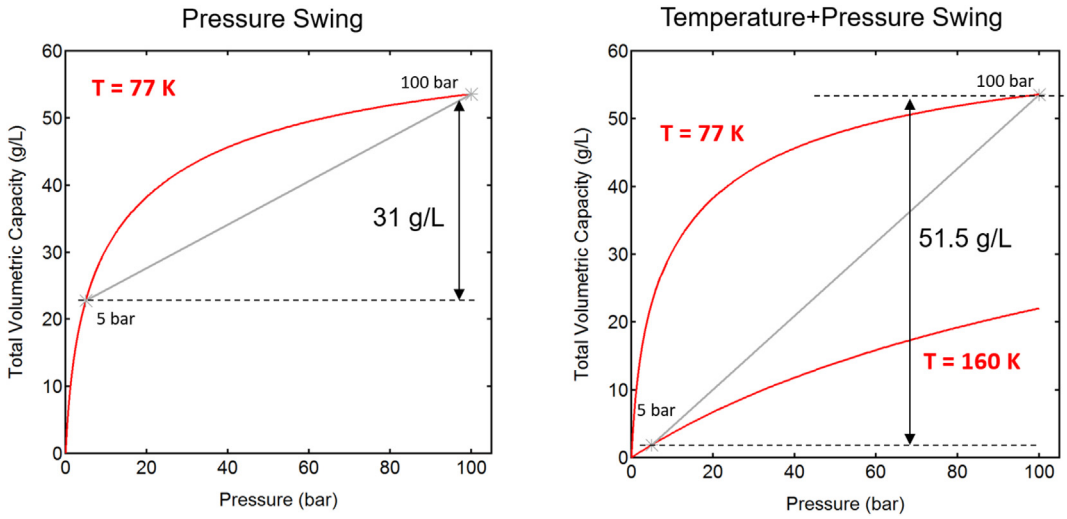

Fig. 1 – Two definitions of material-level H_2 storage capacity for MOF adsorbents. (left) Pressure swing (PS) between 100 bar and 5 bar at 77 K. (right) Temperature plus pressure swing (TPS) between 100 bar, 77 K and 5 bar, 160 K. MOF-5 data is used as the example, with a crystal density of $\rho_{crys} = 0.605$ gcm^{-3} and data from Ref. [22].

Results

Usable hydrogen capacity at 77 K

Computational screening has identified MOFs which surpass the usable PS capacity of MOF-5 at 77 K [13,16,21]. Within this list of candidates, many were successfully synthesized here, including IRMOF-20, SNU-70, NH2-MOF-177, DUT-23 (Co), UMCM-9 and NU-100. While IRMOF-20 and SNU-70 possess the same zinc cluster secondary building unit as MOF-5, and exhibit an equivalent cubic topology, they possess slightly longer organic linkers compared to the 1,4-benzene-dicarboxylic acid linker for MOF-5. This results in larger pore sizes and slightly lower 77 K hydrogen adsorption at low pressures. Despite the crystal density of IRMOF-20 (0.51 gcm^{-3}) and SNU-70 (0.405 gcm^{-3}) being slightly lower than that of MOF-5 (0.605 gcm^{-3}), their isothermal PS volumetric capacity at 77 K actually surpasses that of MOF-5.

The mixed-linker metal-organic framework material UMCM-9 contains two linkers joined through the same zinc cluster, with a similar orthogonal geometry as MOF-5, IRMOF-20 and SNU-70. Despite its low crystal density of 0.37 gcm^{-3}, UMCM-9 has a PS usable volumetric capacity which exceeds that of IRMOF-20 and SNU-70. DUT-23 (Co) has a high excess H_2 adsorption quantity at 77 K, but it does not surpass MOF-5 in PS-usable volumetric capacity. With a low crystal density of 0.291 gcm^{-3}, NU-100 has both the highest excess gravimetric adsorption at 77 K, along with the highest PS usable volumetric capacity at 77 K. Fig. 2 summarizes the excess 77 K H_2 adsorption isotherms, and the volumetric and gravimetric total H_2 storage based on each MOF's ideal crystal density. Additional properties of the characterized MOFs are included in the Supporting Information.

BET surface area versus H_2 excess adsorption

Hydrogen adsorption isotherms at 77 K were measured for MOFs that were stable after activation and possessed a sufficiently large BET surface area (generally >2500 m^{2}g^{-1}). In addition to these MOFs, a number of reference samples were also characterized to supplement these MOFs. These include two readily-synthesized MOFs (UiO-66, UiO-67), MOFs available commercially (Ni-MOF-74, MIL-101-NH2, MOF-177, ZIF-8, HKUST-1), and activated carbons (Norit ROW, MSC-20, MSC-30).

A graphical summary of the adsorbents characterized during this work is provided in Fig. 3. The *y*-axis corresponds to the excess H_2 adsorption at 35 bar and 77 K measured for each sample. The *x*-axis provides the BET specific surface area that was determined from N_2 adsorption isotherms at 77 K. The measured data is consistent with published empirical correlation for MOFs [30]. This supports both the accuracy of the excess H_2 measurements, as well as quality of the synthesized MOF materials. Notably, for MOFs with a BET surface area above 4000 m^{2}g^{-3}, the correlation between surface area and excess H_2 uptake is significantly smaller, and deviates notably from the frequently used 1 wt% per 500 m^{2}g^{-1} correlation.

Hydrogen storage between 80 K and 160 K

Volumetric temperature-pressure swing (TPS) capacities were measured for the highest performing MOFs, following the definition illustrated in the right panel of Fig. 1. These TPS capacities are input for the system-level model used to estimate the gravimetric and volumetric capacity. The default lower and upper temperatures for the system model are 80 K (not 77 K) and 160 K, but there was no temperature control capability to maintain these temperatures experimentally.

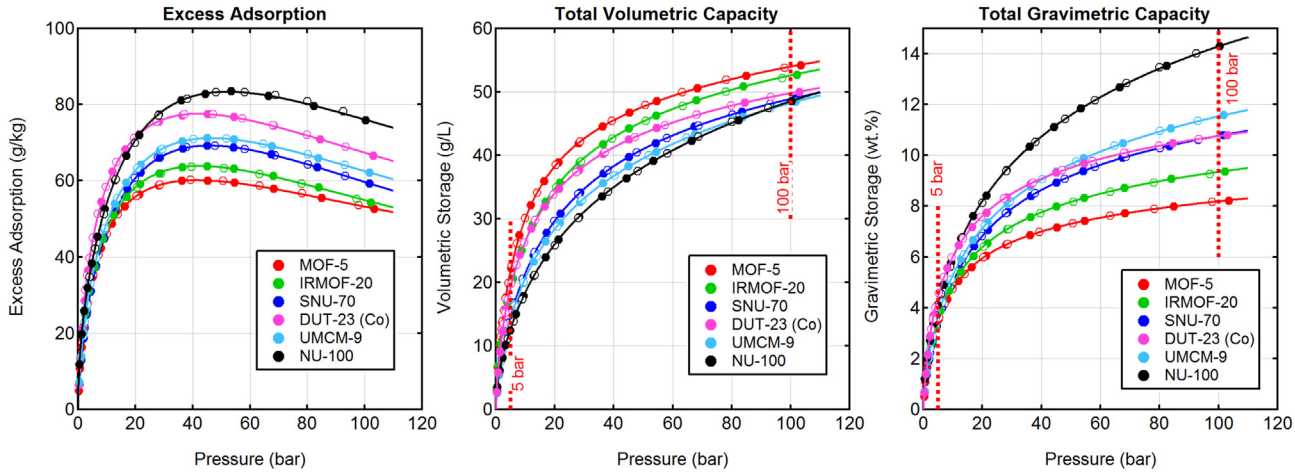

Fig. 2 – (left) Excess H_2 gravimetric adsorption isotherms measured at 77 K for the top performing synthesized MOFs. Adsorption points are plotted as filled markers and desorption points as unfilled markers. (center) Total volumetric storage at 77 K based on each MOF's crystal density. (right) Total gravimetric H_2 storage at 77 K based on crystal density.

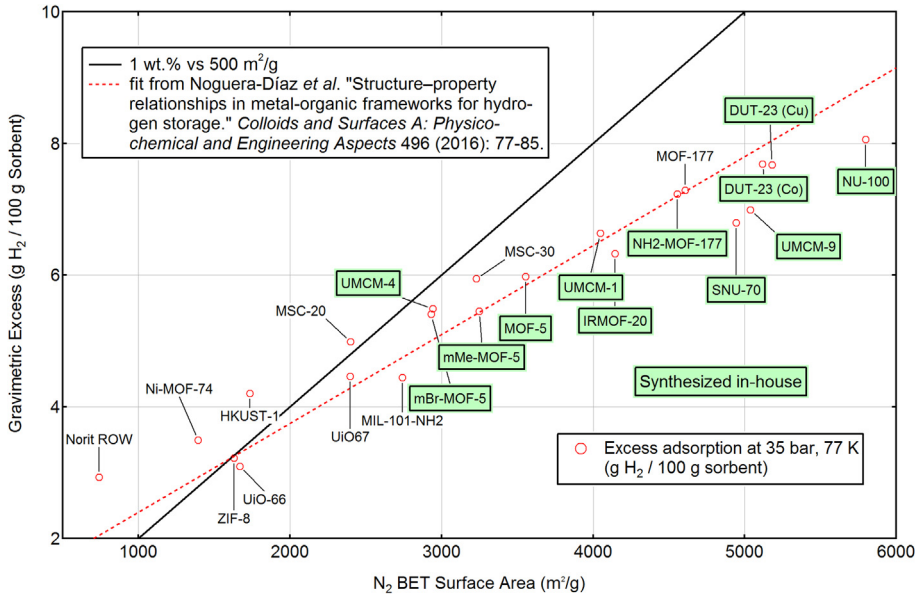

Fig. 3 – Measured excess H_2 adsorption at 35 bar and 77 K plotted versus the measured N_2 BET specific surface area. MOFs synthesized by the authors for this study are highlighted in green. The standard 1 wt% per 500 m^2g^{-1}rule-of-thumb correlation is plotted as a solid black line. A more recent empirical correlation from Ref. [30] is plotted as dashed red line. (For interpretation of the references to colour in this figure legend, the reader is referred to the Web version of this article.)

Instead, isotherms were measured at 77 K, 87 K, 195 K and 297 K, and the 80 K and 160 K isotherm were estimated from the modified Dubinin-Astakhov (D-A) model [31].

$$n_{ex} = n_{max}\exp\left[-\left(\frac{RT}{a+bT}\right)^2 \ln\left(\frac{p_0}{p}\right)^2\right] - \rho_g v_a \quad (4)$$

The modified D-A model is implemented within the system-level analysis to describe the temperature-pressure-composition properties of H_2 uptake in MOFs, as described in greater detail Ref. [14]. While there are difficulties in fitting the modified D-A model to MOF-5 and similar MOFs [22], the quality of fits are sufficient for describing hydrogen storage capacity within the temperature range explored here. Model parameters were not constrained during non-linear optimization. Parameters which produced the best fits to the data were chosen, regardless of whether those values were feasible from a literal interpretation of the physical property that the parameter describes. Hydrogen adsorption isotherms measured at variable temperatures, together with fits to the modified D-A model, are available for MOF-5, IRMOF-20, SNU-70, UMCM-9 and NU-100 in the Supporting Information.

Calculated volumetric storage amounts at 80 K and 160 K for the highest-performing MOFs are summarized in Fig. 4, with the volumetric capacity based on the crystal density of

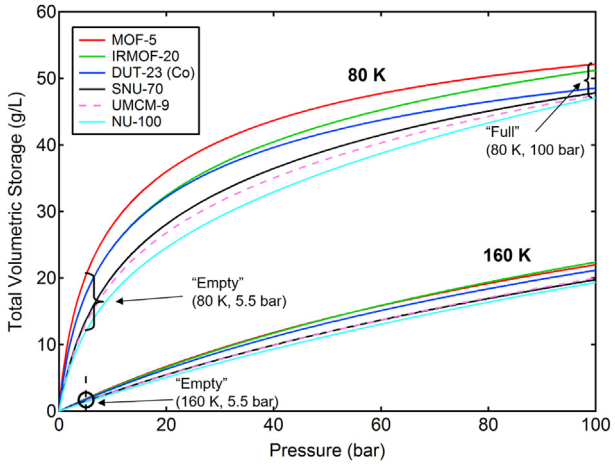

Fig. 4 – Total volumetric hydrogen storage calculated at 80 K and 160 K using fits to the modified D-A model. Hydrogen storage densities are calculated based the crystal density of each individual MOF. The full state (100 bar, 80 K) for both PS and TPS capacities is indicated. Similarly, the empty state for the PS capacity (5 bar, 80 K) and for the TPS capacity (5 bar, 160 K) are indicated.

each MOF. There is a comparatively large variation in the empty state for the 80 K PS capacity (80 K, 5 bar) for the MOFs in Fig. 4. In contrast, the empty state for the TPS capacity (5 bar, 160 K) exhibits little variation for the MOFs included in the plot. Therefore, the TPS capacity is determined primarily by the full state at 80 K and 100 bar. It is notable that MOFs which beat MOF-5 in terms of 77 K PS capacity actually have a lower 80 K/160 K TPS capacity compared to MOF-5. Indeed, the baseline material MOF-5 actually has the highest TPS capacity on a crystal density basis [21].

System model

The HSECoE designed and built two sub-scale prototypes of cryo-adsorption hydrogen storage systems using MOF-5 as the adsorbent [9]. These prototypes were used to develop a model that calculates the gravimetric and volumetric system-level capacities for a full scale 5.6 kg cryo-adsorbent system. Complete details of the system model have been published in Ref. [14].

Fig. 5 provides a schematic of the full-sized cryo-adsorbent system used for the system capacity estimates. To minimize costs, and also to reduce system mass and volume, only a single-tank design is considered in the model. The system utilizes a low-cost type 1 tank made of 6061-T6 aluminum alloy. By keeping the gas pressure below 100 bar, the type-1 tanks can be used instead of type-3 tanks without adding significant additional weight [14]. The tank exterior is wrapped with multi-layer vacuum insulation (MLVI), while the interior of the tank houses a lightweight honeycomb-shaped aluminum heat exchanger which contains holes for cross-sectional hydrogen flow. A benefit of a type-1 tank is that there is no hydrogen permeation through the metal shell, and no out-gassing of volatile organic compounds (which occurs for carbon fiber composite), both of which are known to degrade the vacuum of the MLVI layer [32].

The outer shell contains a a layer of embedded liquid N_2 channels to help cool the type-1 tank rapidly during refueling, and an additional 2 mm aluminum outer shell for dormancy and protection purposes. The balance of plant includes an on-tank valve, a refueling receptacle, a pressure regulator, and a heat exchanger element that warms the dispensed hydrogen using the fuel cell coolant loop before it enters the FC stack. Additional balance-of-plants (BOP) components are described in Ref. [14]. Due to the scarcity of commercially available balance-of-plant components that are designed for the operating conditions required for a cryo-adsorbent system, assumptions about their attributes (particularly mass, volume) may be overly-conservative.

The system is cooled to its base temperature through the combination of a liquid nitrogen cooling loop layer around the outside of the tank, and by re-circulating cold hydrogen gas (at 77 K) through the tank interior. Hydrogen gas is dispensed at roughly 77 K from a cryogenic pump at the forecourt, and is supplied from a liquid hydrogen tank. These cool-down procedures also help to dissipate the moderate heat of H_2 adsorption, which is around 3–5 kJ/mol·H_2 for the MOFs studied in this project (see Supporting Information for comparisons of the isosteric heats). Heat transfer issues in MOF-5-based sub-scale systems have been reported previously [33–35].

When MOFs are packed to a high density, hydrogen gas flow-through-cooling may no longer be effective. Therefore, there has also been work on a different type of sub-scale prototype tank that houses high-density compacted MOF monoliths separated by heat spreader plates containing internal liquid N_2 micro-channels [36]. This alternative tank architecture is not considered in the system model estimates presented here.

Some system attributes are fixed based on operating conditions and material properties. For example, the tank wall thickness is determined by material tensile strength, pressure range, temperature range, and tank design (type-1, or type-3). Similarly, the heat exchanger size limited by the heat capacity and heat transfer properties of the highly-insulating MOF powders (which potentially could be mixed with conductive additives like graphite) [35].

A number of the system attributes can be adjusted, and potentially optimized. Using MOF-5 as the adsorbent, Ref. [14] previously reported the results of a sensitivity analysis of temperature and MOF-5 density on the overall system capacity. Conservative values for the full state and empty state are 100 bar/80 K and 5.5 bar/160 K, respectively. Lowering the full state temperature from 80 K to 77 K without increasing cool-down time is a challenge, due to heat transfer throughout the insulated tank. Raising the upper *empty* temperature above 160 K would also increase the refueling time needed to bring the temperature back down to the base value (although a more detailed study of cool-down time versus increased capacity as a function of temperature limits would be valuable) [14].

The MLVI insulation thickness is set to 23 mm as a conservative initial value, but thicknesses as thin at 10 mm have been demonstrated for cryo-compressed H_2 storage systems [32]. Additionally, changing the type-1 tank material from Al alloy to 316 stainless steel can improve volumetric capacity

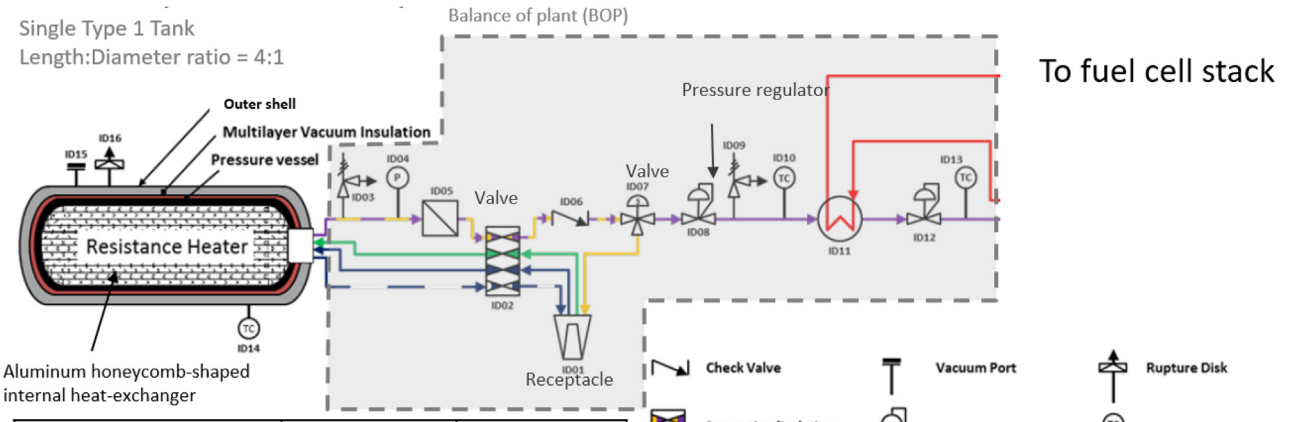

	Initial	Optimized
Initial/Full Pressure:	100 bar	
Initial/Full Temperature:	80 K	77 K
Final/Empty Pressure:	5.5 bar	
Final/Empty Temperature:	160 K	
Useable Hydrogen	5.6 kg	
Pressure Vessel Type	Type 1	
Pressure Vessel Material	Alluminum Alloy	Stainless Steel
Insulation Thickness	23 mm	10 mm
LN_2 Chiller Channel	3/8 inch	1/4 inch

Fig. 5 – Schematic of a full-scale cryo-adsorbent hydrogen storage system designed for a 5.6 kg usable capacity. Adjustable system attributes are indicated in the system properties table at the lower left. Values in the column labeled Initial were the default values used for system modeling results. The system parameters in the column labeled Optimized can be realistically achieved through engineering improvements. The impact of the optimized parameters on system capacity is explored in the Strategies to improve system capacity section. Figure is adapted from Ref. [14].

due to thinner tank walls, although increasing cost and weight. Lastly, the material-level H_2 storage properties of each MOF were determined by adsorption measurements as described in Usable hydrogen capacity at 77 K, and were considered as non-adjustable parameters for a given adsorbent material.

System-level storage capacities are impacted by the MOF packing density within the tank. Not only does this adjustable parameter dictate the fraction of internal volume that is void space versus MOF-occupied space, it can alter the integrity of the MOF pore structure. While lightly tapping down a loosely packed MOF powder will not necessarily generate this effect, mechanically compacting the MOF powder to densities approaching the crystal density (using a pellet press for example) may induce degradation to the pore structure, reducing both pore volume and hydrogen adsorption capacity [37].

The characterization of the compaction properties of the top performing MOFs are presented in the next section.

MOF powder packing

To accurately model the effect of MOF packing density on the system level capacity, it was necessary to develop a transfer function that captures the effect of mechanical compaction on the hydrogen storage density of MOFs. Measurements were performed for a subset of the top-performing MOFs to quantify the effect of mechanical compaction on the hydrogen adsorption capacity at 77 K. Selected measurements are provided in Fig. 6, which shows the excess H_2 adsorption isotherms for SNU-70, MOF-177, and MOF-5 after compacting a powder sample to successively higher densities.

As expected in Fig. 6, excess H_2 adsorption amounts decrease as the MOFs are compacted to higher densities. It may be possible to improve the compaction efficiency through the addition of lubricants or particle size control, although there is little data in the literature to assess the effectiveness of these strategies. An additional approach is to compact the MOF before the activation step, while pores are filled with solvent, which may provide additional support against framework compression or shear [38].

The modified D-A model parameters used to describe material-level hydrogen storage capacities must be scaled down to capture the mechanical degradation effect. An approximate method was utilized to correlate a unit-less degradation factor for each MOF with a unit-less compaction parameter. Firstly, the mechanical degradation parameter is defined as the ratio of the maximum 77 K excess H_2 adsorption

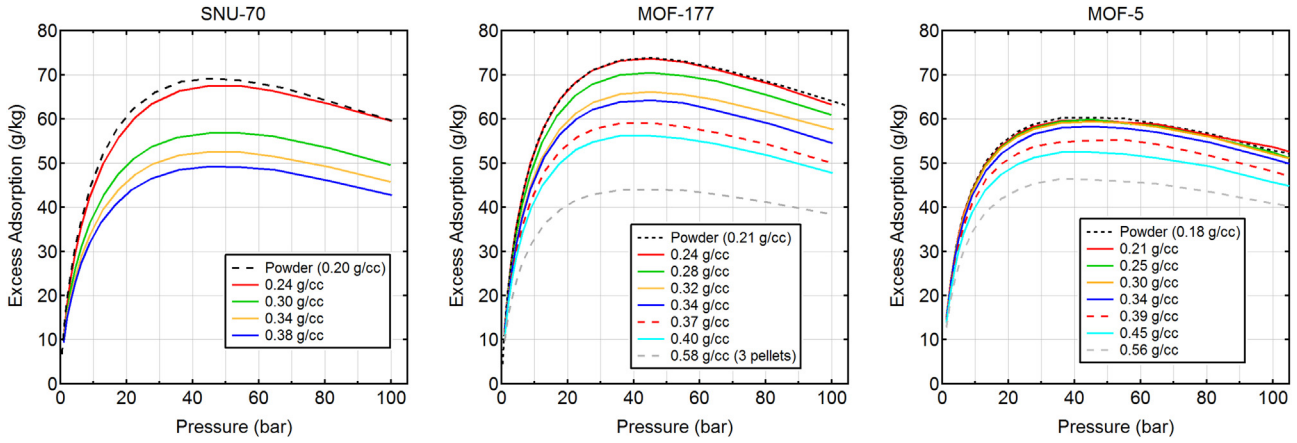

Fig. 6 – Excess H_2 adsorption isotherms measured at 77 K for SNU-70 (left), MOF-177 (center) and MOF-5 (right), after compacting MOFs to specified densities. The powders were densified by uniaxial compaction directly inside the sample cell using a manual pellet press.

at a particular MOF density against its maximum excess adsorption as a powder. Second, the compaction parameter is defined as the packing density (ρ_x) divided by the MOF crystal density. The correlation between these two parameters is displayed in Fig. 7.

The compaction-induced capacity loss for MOF-5, MOF-177, SNU-70 and NU-100 appear to follow a similar trend in Fig. 7. Hydrogen excess adsorption retains its full capacity up to a density of approximately 50% of the crystal density. At that point the maximum excess adsorption value starts to decrease with continued mechanical compaction. The empirical trend for the combined data set of all three MOFs shown in Fig. 7 can be approximated as,

$$\mathrm{Y} = \frac{n_{ex}^{max}\{\text{compacted}\}}{n_{ex}^{max}\{\text{powder}\}} = \begin{cases} 1 & \text{if } \frac{\rho_{pack}}{\rho_{crys}} < 0.519 \\ 1.32 - 0.616 \times \left(\frac{\rho_{pack}}{\rho_{crys}}\right) & \text{if } \frac{\rho_{pack}}{\rho_{crys}} > 0.519 \end{cases} \quad (5)$$

Where the left-hand-side equals the ratio of the maximum excess adsorption of the compacted MOF at density ρ_{pack} and the maximum excess adsorption for the powder MOF at density ρ_{pwd}. The ratio of H_2 adsorption for compacted versus powder MOFs can then be used to apply D-A parameters measured for the powder sample to a system in which the MOF has been compacted beyond its powder density. In this case, two of the D-A model parameters are transformed by multiplying by a pre-factor Y,

$$n_{max}^{*} = \mathrm{Y} \times n_{max} \qquad v_a^{*} = \mathrm{Y} \times v_a \quad (6)$$

which can then be substituted back into Eq. (4) to scale the modified D-A model for compaction-induced capacity loss.

System-level capacity versus MOF density

Modified D-A parameters were measured for powder samples of MOF-5, MOF-177, IRMOF-20, DUT-23(Co), SNU-70 and NU-100, as described in Sec. 3.3. Using Eqs. (5) and (6), system-level hydrogen storage capacities were calculated for these MOFs at densities above their powder packing density. Baseline values for system parameters such as pressure and temperature ranges, insulation thickness, and tank type are described in the System model section and in Fig. 5. The results of the system-level estimates are shown in Fig. 8.

Based on real MOF powder packing behavior, MOF-5 ultimately attains the highest volumetric capacity at the system level when it is compacted to a density between 0.4 gcm^{-3} and 0.5 gcm^{-3}. At these high densities, however, rapid flow-through cooling of the sorbent media may not be realistically achievable. At a lower packing such as 0.2 gcm^{-3}, closer to what would be obtained for a bulk powder, MOFs with lower crystal density yield a higher volumetric capacity than MOF-5.

The optimum MOF for the cryo-adsorbent system therefore depends on the MOF packing density, which itself may be restricted by both the system architecture and by methods for

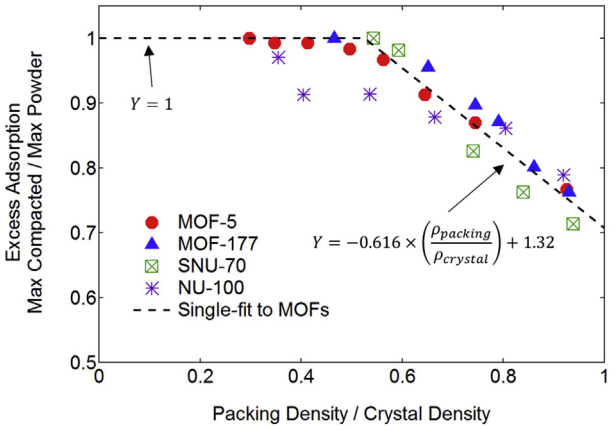

Fig. 7 – Mechanical degradation of MOF versus compaction density. The y-axis corresponds to the ratio between the maximum excess adsorption at 77 K for a MOF compacted to a specific density divided by the value for the initial value measured for the powder. The *x*-axis corresponds to the density of the compacted MOF divided by its crystal density.

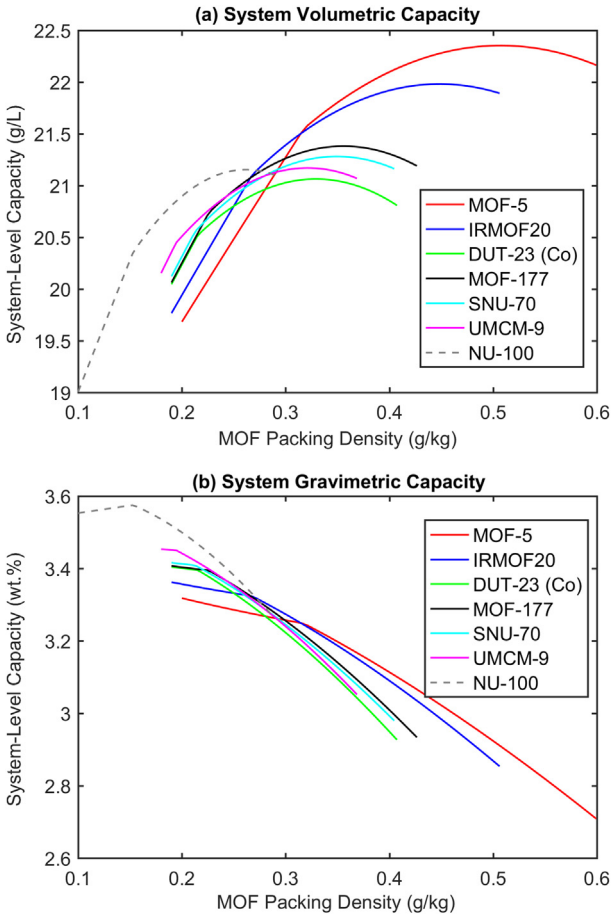

Fig. 8 – Usable volumetric hydrogen storage capacity for MOFs at the system-level when compacted above their powder packing density. (a) Volumetric capacity in g/L versus compaction density of MOFs. (b) Gravimetric capacity in wt% versus compaction density of MOFs. Values are calculated based on the default, non-optimized, system parameters.

loading and compacting the MOF powder within the tank. Alternate system designs (such as the MATI design described in Ref. [36]) would be required at high MOF packing fractions to address lower H_2 permeability rates through dense MOF monoliths. In this case development of a monolith version of the system model would better capture the performance at high MOF densities. From panel (b) in Fig. 8, it is clear that increasing the MOF density generally causes the system-level gravimetric capacity to decrease due to the addition of additional mass from the MOF. The increase in volumetric capacity should be balanced against the corresponding decrease in gravimetric capacity.

How material-level capacity translates to system-level capacity

One goal of this study was to better understand how material-level hydrogen storage properties translate to system-level performance. Referring to Fig. 2, the baseline material (MOF-5) has a maximum excess hydrogen adsorption of 60.0 g/kg at 77 K. Meanwhile, the maximum excess adsorption for DUT-23 (Co) was measured at 77.6 g/kg, a nearly 30% increase. However, such large increases in material level gravimetric storage do not translate into significant increases in gravimetric or volumetric capacity at the system level.

Fig. 9 illustrates the weak correlation between material-level excess hydrogen adsorption and system-level hydrogen storage capacity for a powder-based system. On the x-axis, the maximum excess hydrogen adsorption measured for each MOF is expressed as a percent change versus that of MOF-5. The y-axis indicates the system-level capacities for each MOF at a representative powder packing density, which is assumed to be equal to one half of the crystal density (Referring back to Fig. 7, this is the density that many MOFs can be compacted to without degrading the hydrogen adsorption.). The system-level gravimetric capacity (red circles) increases with increasing excess adsorption, but the gains are relatively modest. On the other hand, system-level volumetric capacity (blue triangles) actually decreases going from MOF-5 to NU-100, due primarily to the lower packing density.

Strategies to improve system capacity

The system-level storage capacities presented in Fig. 8 remain below the 2020 DOE target of 30 g/L, and do not match the typical volumetric capacities for a 700 bar compressed system (25 g/L). This deficiency largely reflects the impact of the system mass and volume, as the material-level values can surpass their respective targets.

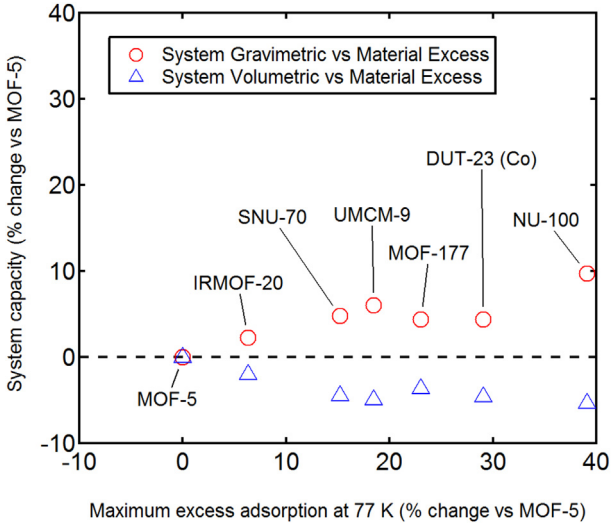

Fig. 9 – Correlation between material level storage and system-level H_2 storage capacities. The bottom axis is the maximum excess gravimetric H_2 adsorption at 77 K for the indicated MOFs, expressed as a percent change versus MOF-5. The left axis is the system-level gravimetric (red circles) and volumetric (blue triangles) hydrogen storage capacity at the powder packing density for each MOF, defined here as the half the MOF crystal density. It is expressed as the percent change versus MOF-5. (For interpretation of the references to colour in this figure legend, the reader is referred to the Web version of this article.)

However, there are a number of opportunities for improving the capacity of the cryo-adsorbent hydrogen storage system. These improvements include:

- Switching the type-1 tank material from aluminum alloy to 316 stainless steel. This reduces wall thickness and saves volume at the expense of increased cost.
- Reducing the MLVI thickness from 23 mm to 10 mm. Prototype cryo-compressed H_2 storage tanks have demonstrated the feasibility of MLVI thicknesses as thin as 10 mm. Because the insulation is pivotal to the dormancy performance of the cryo-adsorbent system, this would require extensive optimization and validation. If implemented, this could significantly reduce the outer volume of the tank.
- Reducing the liquid nitrogen cooling channel thickness from 3/8 inch to 1/4 inch. This would help to reduce the outer volume of the tank assembly.
- Lower the baseline fill temperature from 80 K to 77 K. This may be technically feasible with an optimized cool-down procedure which utilizes both an external LN2 loop and internal recirculation of pre-cooled 77 K hydrogen gas. Even a small decrease in temperature can increase amount of hydrogen gas that can be loaded into the tank.
- Lastly, methods of synthesizing MOFs as high density monoliths without the corresponding mechanical degradation and decrease in H_2 adsorption are an area of active research [39]. Below, we explored the possibility of compacting a MOF to its crystal density without any deterioration in its hydrogen adsorption.

The effects of these improvements on the system-level volumetric capacity are depicted as a waterfall chart in Fig. 10. The starting quantity is simply the outer volume for an empty single-tank cryo-adsorbent system (no MOF loaded) which has an internal volume needed to store 5.6 kg of hydrogen gas at 77 K and at 100 bar. Next, the required outer volume of the system is calculated when the tank is filled with powder MOF-5 at a conservative packing density of 0.13 gcm^{-3} [15]. Storing the same 5.6 kg of usable hydrogen gas, the external volume of the system decreases by 41 L due to the enhanced storage density of the MOF-5. Next, the MOF material is switched from MOF-5 to UMCM-9 packed at a moderate density of 0.2 gcm^{-3}. (UMCM-9 is chosen here rather than NU-100, because it has not been studied as extensively as the latter material). The external volume now decreases by an additional 28 g/L due to the increased storage capacity of UMCM-9 at 0.2 gcm^{-3}.

Next, the effect of the system engineering improvements itemized above is considered in Fig. 10. These improvements include reducing the MLVI thickness, reducing the LN2 cooling channel thickness, and lowering the baseline fill temperature. These simple optimizations lead to a surprisingly large decrease in the required system volume of about 68 L, sufficient to surpass the 25 g/L baseline capacity of a typical 700 bar compressed storage system.

The last hypothetical improvement comes from compacting the UMCM-9 powder to its crystal density ($\rho_{crys} = 0.37$ gcm^{-3}) with no resulting decrease in excess adsorption (i.e., not including the degradation shown in Fig. 7). This trims off an additional 20 L of external system volume, such that the final volumetric system capacity is over 30 g/L. This highlights the importance of developing a compaction method which does not induce mechanical degradation to the MOF pore structure. Strategies for optimizing MOF powder compaction include engineering the crystallite size and shapes, along with minimizing friction sources during mechanical compaction.

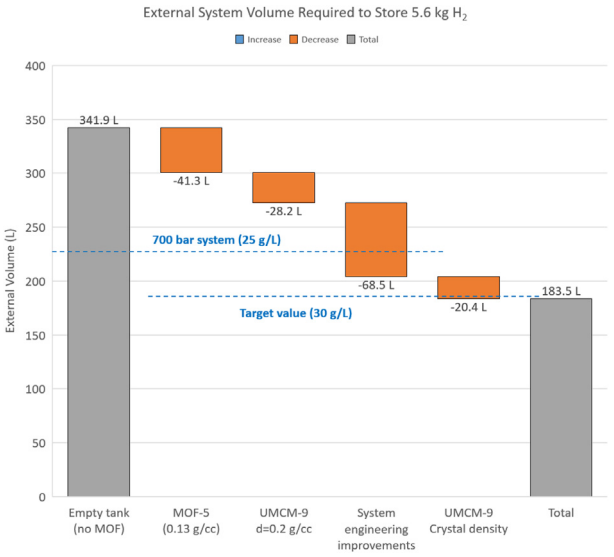

Fig. 10 – Waterfall chart depicting the total external system volume required to store 5.6 kg of usable hydrogen gas. Starting from an empty tank storing hydrogen gas at 77 K and 100 bar, the reduction in external volume is shown for each modification to the system. Engineering improvements (described in Strategies to improve system capacity) include reducing the MLVI thickness, reducing the LN2 cooling channel thickness, and lowering the baseline fill temperature.

Conclusion

In this study we have evaluated the hydrogen adsorption properties for a number of high-surface-area MOFs identified through computational screening as having the potential of surpassing MOF-5 in both volumetric and gravimetric storage capacity. Additionally, the effect of MOF compaction density on their hydrogen storage capacity was characterized. These measurements were utilized to estimate the hydrogen storage capacities at the system-level for MOFs which demonstrated a high volumetric and gravimetric H_2 storage density. System estimates were based on a single tank cryo-adsorbent system that utilizes a type-1 aluminum tank, with multi-layer vacuum insulation, liquid N_2 cooling channels, in-tank heat exchanger, and a packed MOF powder inside the tank. It was found that MOFs with ultra-high gravimetric surface areas and hydrogen adsorption amounts do not necessarily yield high volumetric (or even gravimetric) storage capacities at the system-level. Meanwhile, attributes such as powder compaction efficiency and sorbent bed temperature were

shown to have a large impact on the amount of hydrogen that is stored within a fixed system volume.

Acknowledgements

Financial support for this study was provided by the US Department of Energy, Office of Energy Efficiency and Renewable Energy, Grant no. DE-EE0007046.

Appendix A. Supplementary data

Supplementary data to this article can be found online at https://doi.org/10.1016/j.ijhydene.2019.04.082.

REFERENCES

[1] Yang J, Sudik A, Wolverton C, Siegel DJ. Chem Soc Rev 2010;39:656–75.
[2] Broom D, Webb C, Hurst KE, Parilla PA, Gennett T, Brown CM, Zacharia R, Tylianakis E, Klontzas E, Froudakis G, et al. Appl Phys A 2016;122:151.
[3] U.S. DRIVE. Hydrogen delivery technical team, hydrogen delivery technical team roadmap. Technical Report; 2017.
[4] Murray LJ, Dincă M, Long JR. Chem Soc Rev 2009;38:1294–314.
[5] Beckner M, Dailly A. Int J Energy Res 2016;40:91–9.
[6] Czaja AU, Trukhan N, Müller U. Chem Soc Rev 2009;38:1284–93.
[7] Silva P, Vilela SM, Tomé JP, Paz FAA. Chem Soc Rev 2015;44:6774–803.
[8] Li H, Eddaoudi M, O'Keeffe M, Yaghi OM. Nature 1999;402:276.
[9] Siegel DJ, Hardy B. Engineering an adsorbent-based hydrogen storage system: what have we learned?. Technical report. Golden, CO: Hydrogen Storage Summit; 2015. https://energy.gov/sites/prod/files/2015/02/f19/fcto_h2_storage_summit_siegel.pdf.
[10] Farha OK, Yazaydın AÖ, Eryazici I, Malliakas CD, Hauser BG, Kanatzidis MG, Nguyen ST, Snurr RQ, Hupp JT. Nat Chem 2010;2:944.
[11] Furukawa H, Ko N, Go YB, Aratani N, Choi SB, Choi E, Yazaydin AÖ, Snurr RQ, O'Keeffe M, Kim J, et al. Science 2010;329:424–8.
[12] Farha OK, Eryazici I, Jeong NC, Hauser BG, Wilmer CE, Sarjeant AA, Snurr RQ, Nguyen ST, Yazaydın AO, Hupp JT. J Am Chem Soc 2012;134:15016–21.
[13] Goldsmith J, Wong-Foy AG, Cafarella MJ, Siegel DJ. Chem Mater 2013;25:3373–82.
[14] Tamburello D, Hardy B, Corgnale C, Sulic M, Anton D, in: ASME 2017 Fluids Engineering Division Summer Meeting, American Society of Mechanical Engineers, pp. V01BT08A005–V01BT08A005, https://doi.org/10.1115/FEDSM2017-69411.
[15] Veenstra M, Yang J, Xu C, Purewal J, Gaab M, Arnold L, Müller, Siegel D, Ming Y. U.S. Department of Energy Hydrogen and Fuel Cells Program Annual Merit Review Proceedings. 2015.
[16] Ahmed A, Liu Y, Purewal J, Tran LD, Wong-Foy AG, Veenstra M, Matzger AJ, Siegel DJ. Energy Environ Sci 2017;10:2459–71.
[17] Eddaoudi M, Kim J, Rosi N, Vodak D, Wachter J, O'keeffe M, Yaghi OM. Science 2002;295:469–72.
[18] Prasad TK, Suh MP. Chem–Eur J 2012;18:8673–80.
[19] Klein N, Senkovska I, Baburin IA, Gruenker R, Stoeck U, Schlichtenmayer M, Streppel B, Mueller U, Leoni S, Hirscher M, et al. Chem–Eur J 2011;17:13007–16.
[20] Koh K, Van Oosterhout JD, Roy S, Wong-Foy AG, Matzger AJ. Chem Sci 2012;3:2429–32.
[21] Ahmed A, Seth S, Purewal J, Wong-Foy AG, Veenstra M, Matzger AJ, Siegel DJ. Nat Commun 2019;10(1):1568.
[22] Purewal J, Liu D, Sudik A, Veenstra M, Yang J, Maurer S, Müller U, Siegel D. J Phys Chem C 2012;116:20199–212.
[23] Thommes M, Kaneko K, Neimark AV, Olivier JP, Rodriguez-Reinoso F, Rouquerol J, Sing KS. Pure Appl Chem 2015;87:1051–69.
[24] Walton KS, Snurr RQ. J Am Chem Soc 2007;129:8552–6.
[25] Yunes S, Wommack P, Still M, Kenvin J, Exley J. Appl Catal Gen 2014;474:250–6.
[26] Broom D, Webb C. Int J Hydrogen Energy 2017;42:29320–43.
[27] Parilla PA, Gross K, Hurst K, Gennett T. Appl Phys A 2016;122:201.
[28] Mason JA, Veenstra M, Long JR. Chem Sci 2014;5:32–51.
[29] Schlichtenmayer M, Hirscher M. Appl Phys A 2016;122:379.
[30] Noguera-Díaz A, Bimbo N, Holyfield LT, Ahmet IY, Ting VP, Mays TJ. Colloids Surf, A 2016;496:77–85.
[31] Richard M-A, Bénard P, Chahine R. Adsorption 2009;15:43–51.
[32] Aceves SM, Petitpas G, Espinosa-Loza F, Matthews MJ, Ledesma-Orozco E. Int J Hydrogen Energy 2013;38:2480–9.
[33] Ubaid S, Zacharia R, Xiao J, Chahine R, Bénard P, Tessier P. Int J Hydrogen Energy 2015;40:9314–25.
[34] Hou XX, Sulic M, Ortmann JP, Cai M, Chakraborty A. Int J Hydrogen Energy 2016;41:4026–38.
[35] Ming Y, Chi H, Blaser R, Xu C, Yang J, Veenstra M, Gaab M, Müller U, Uher C, Siegel DJ. Int J Heat Mass Transf 2015;82:250–8.
[36] Drost K, Jovanovic G, Paul B. Microscale enhancement of heat and mass transfer for hydrogen Energy storage. Technical Report, Final Technical Report; 2015.
[37] Purewal J, Liu D, Yang J, Sudik A, Siegel D, Maurer S, Müller U. Int J Hydrogen Energy 2012;37:2723–7.
[38] Xu C, Purewal J, Veenstra MJ. Solvent-supported compaction of metal-organic frameworks. US Patent 2017;9. 757,710.
[39] Tian T, Zeng Z, Vulpe D, Casco ME, Divitini G, Midgley PA, Silvestre-Albero J, Tan J-C, Moghadam PZ, Fairen-Jimenez D. Nat Mater 2018;17:174.